Chemical Engineering Science 126 (2015) 267–282

Contents lists available at ScienceDirect

Chemical Engineering Science

journal homepage: www.elsevier.com/locate/ces

Investigating the interactions between physical and biological heterogeneities in bioreactors using compartment, population balance and metabolic models

Maxime Pigou, Jérôme Morchain *

Université de Toulouse, Laboratoire d'Ingénierie des Systèmes Biologiques et des Procédés, INSA/CNRS/INRA, 135 Avenue de Rangueil, 31077 Toulouse Cedex, France

HIGHLIGHTS

- Population balance, metabolic and compartment models are coupled.
- The disequilibrium between substrate uptake and utilization rate is introduced.
- Simulations at lab and large scales compare favorably to *E. coli* culture data.
- Mixing limitation induces substrate gradients affecting metabolism.
- Through scale-up, yield loss and by-product formation are predicted.

GRAPHICAL ABSTRACT

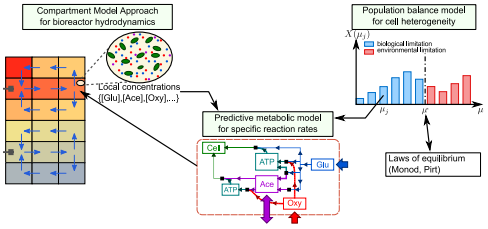

ARTICLE INFO

Article history:
Received 21 July 2014
Received in revised form
3 November 2014
Accepted 14 November 2014
Available online 26 November 2014

Keywords:
Two-way coupling
Population balance
Metabolic model
Compartment model
Bioreactor scale-up

ABSTRACT

A generic model for the description of biological population dynamics in industrial bioreactors is detailed. Hydrodynamics, mass transfer between the cell and the surrounding fluid, population heterogeneity, metabolism and biological adaptation have to be considered with equal interest and, if possible, simultaneously. This model couples a hydrodynamic model, a population balance model for the growth rate adaptation and a metabolic model predicting the reaction rates depending on the state of the individuals. This approach dissociates the growth rate from local concentrations leading to a good understanding of the effects of a changing environment on a microbial population. Our model is applied to *Escherichia coli* for which experimental data exist in the literature for batch and fed-batch cultures. The considered strain is known for producing acetate when exposed to heterogeneities. When simulating a large bioreactor using a compartment model approach for hydrodynamics, our coupled model could predict that, under certain conditions, acetate is simultaneously produced and consumed in different areas of the reactor.

1. Introduction

The modeling of intensified bioreactors is a current challenge for both the academic and industrial communities. This is principally due to the complexity of such processes that combine mixing, transfer and reaction over a very large range of time and length scales. Compared to other chemical processes, the case of bioprocesses is even more complex because of the dynamic response of biosystems (Enfors et al., 2001). The chemical composition of the liquid phase constraints the cell potential, the biological uptakes modify the concentration fields and microorganisms adapt to the concentration changes experienced along their trajectories. Aiming at higher productivities always pushes the bioreactor towards a more severe competition between mixing and substrate uptake (Linkès et al., 2014). The main consequence is the formation of large scale concentration gradients which in turn expose cells to fluctuating concentration signals further triggering cell

* Corresponding author. Tel.: +33 561559774; fax: +33 561559400.
E-mail address: jerome.morchain@insa-toulouse.fr (J. Morchain).

http://dx.doi.org/10.1016/j.ces.2014.11.035
0009-2509/

adaptation and metabolic dysfunctioning. It has been shown that periodic exposure to excessive substrate concentration induces some modifications of the cell metabolism and leads to: (i) the over assimilation of substrates, (ii) the formation of by-products, and (iii) a decrease in the overall reactor performance. As a result, the modeling and simulation of industrial bioreactors leads to a strong two-way coupling issue illustrated in Fig. 1. Indeed, in biological reactors, the reaction rates co-evolve with concentration fields due to a permanent adaptation of the physiological state of cells.

Comparing the characteristic times of the various processes involved is of great help to identify the potential issues. In a previous work, mixing, substrate uptake and biological adaptation times were considered (Morchain et al., 2014). An important result concerns the concept of local equilibrium between the biophase and the liquid phase. A cell may adapt to any change in its environment (Ferenci, 1996, 1999) through a large variety of response systems having different characteristic times (Wick et al., 2001, 2002; Franchini and Egli, 2006; Ryall et al., 2012). As an illustration, growth rate adaptation is a slow process whereas the change of biovolume due to an osmotic shock is very fast. In between, the characteristic time of substrate uptake regulation is in the range of a few seconds. In most, if not all, studies coupling hydrodynamics and bioreactions, it is assumed that the microorganisms are at an equilibrium with their environment: the reaction rates are calculated from the local concentrations in the liquid phase via a kinetic (Altintas et al., 2006; Peskov et al., 2012) or a metabolic model (Xu et al., 1999; Meadows et al., 2010; Matsuoka and Shimizu, 2013). The consequence is that the actual history of cells is not considered: all cells are supposed to behave as if they were adapted to that local environment. In other words, instantaneous adaptation of the cell functioning is postulated. In order to account for the cell diversity and the ability to be out of equilibrium, the outgoing approach is to consider population balance modeling. Cells are segregated according to one or more internal properties. They are presumably different from one another. The vector of internal properties can be used to define the behavior of any cell in terms of reaction rates. This approach is very powerful to address the issues related to bioreactor dynamics. Unfortunately, cell ensembles (Henson et al., 2002; Mantzaris, 2005, 2006, 2007) and class methods (Lencastre Fernandes et al., 2012) are not easy to implement in the framework of Computational Fluid Dynamics softwares and would lead to prohibitively large computational times (Lapin et al., 2006).

Nevertheless, hydrodynamics, mass transfer between the cell and the surrounding fluid, population heterogeneity, metabolism and biological adaptation have to be considered with equal interest and, if possible, simultaneously. One possibility to combine all these aspects into a tractable model is to reduce the size of the problem through the use of a simplified hydrodynamic model named compartment approach (Vrábel et al., 1999, 2000; Lencastre Fernandes et al., 2013). Bezzo et al. (2003), Moullec et al. (2010) and Delafosse et al. (2014) have proposed different techniques to transpose the 3D-CFD results into a reduced compartment model.

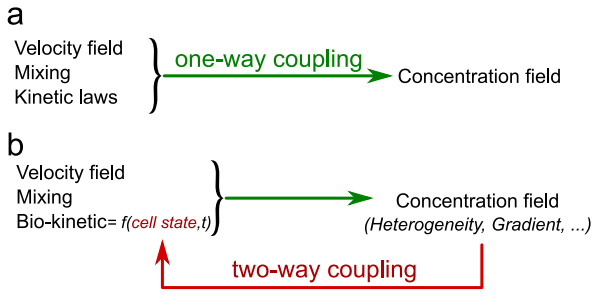

Fig. 1. Illustration of (a) the one-way coupling (as in chemical reactors) and (b) the two-way coupling in biochemical reactors: concentration gradients impact the cell state and induce biological heterogeneity.

In this paper, we propose to combine a compartment model approach for the hydrodynamics, a population balance model for the population dynamics and a metabolic model for the description of bioreactions. The problem formulation is closed by setting the mass transfer law between cells and the liquid phase. The first part of the paper deals with the model presentation with a minimum details since most aspects have already been published elsewhere (Morchain and Fonade, 2009; Morchain et al., 2013, 2014). Then the metabolic part of the model (adapted from Xu et al., 1999) is validated against experimental results obtained in a small scale (15 L) batch cultivation of *Escherichia coli*. In the third part the whole model combining the aforementioned aspects is compared to some experimental results from a 20 m^3 fed-batch cultivation of the same strain (Xu et al., 1999a; Vrábel et al., 2001). In that case, we will rely upon the reactor compartimentation proposed by the authors. A significant improvement of the predictive capacities is obtained with our two-way coupled approach, without parameter adjustment between the two scales. Namely, the occurrence of a disequilibrium between the cell and the environment allow the formation of large amount of by-products when assimilation rates exceed the internal utilization rates for growth and energy production. On the opposite, by-products are uptaken and used as secondary substrate in zones where the main substrate is depleted. Owing to the population balance approach the threshold between substrate excess and substrate limiting conditions is relative to the physiological state of each microorganism. The actual behavior of each subgroup of cells results from the disequilibrium between its own potential and that offered by the local environment.

2. Materials and methods

2.1. Hydrodynamic model

The principle of the Compartment Model Approach (CMA) is briefly recalled hereafter. More details can be found in the original papers of Hristov et al. (2004) and Zahradník et al. (2001). In such a model, the reactor's volume is split into N sub-volumes, referred as "compartments" and considered as perfectly homogeneous. We then need to define a "circulation map" representing the flow pattern circulating between those compartments. This circulation map may be deduced from CFD simulations (Delafosse et al., 2010, 2014) or experimental observations (Vrábel et al., 1999).

To mathematically implement such a model, we define a matrix of volume flow rates, M^f, which is a N-by-N matrix such as the $M^f_{m,n}$ entry of this matrix is the value of the flow, expressed in $m^3.h^{-1}$, going from the m-th compartment to the n-th one with m and $n \in \{1, \ldots, N\}$.

Let C_i^n be the mass concentration of any species, referred as i, in the compartment $n \in \{1, \ldots, N\}$. Then, the mass conservation equation for this species in the n-th compartment is given in the following equation:

$$\frac{\partial C_i^n}{\partial t} = R_i + T_i + \sum_{m=1}^{N} (M^f_{m,n} C_i^m) - C_i^n \sum_{m=1}^{N} (M^f_{n,m}) \quad (1)$$

The term T_i is a gas–liquid transfer rate and R_i an overall reaction rate, both expressed in $g_i\,L^{-1}\,h^{-1}$. The calculation procedure for the bioreaction rates will be detailed in following parts through a population balance model and a metabolic model.

The mass balances, for each species and over each compartment, lead to a set of Ordinary Differential Equations. The ODEs sets were solved using a program written with MATLAB® 7.9 (R2009b) using the ODE solver *ode23* with relative and absolute error tolerances set respectively to 10^{-3} and 10^{-6}.

2.2. Population balance

The population balance model, detailed in previous papers (Morchain et al., 2013, 2014), discriminates individuals depending on their growth capabilities represented by a biological growth rate μ. The application of the general formulation of a Population Balance Equation (PBE) proposed by Ramkrishna (2000), adapted to our case in a homogeneous volume, is given by the following equation:

$$\frac{\partial X(\mu,t)}{\partial t} = -\frac{\partial}{\partial \mu}(X(\mu,t)\zeta) + h(\mu,t) \tag{2}$$

In this formulation, ζ represents the rate of variation of the internal variable μ and h is the rate of production of cell with a given value of μ.

We consider that the cell division will lead to the formation of daughter cells which inherit of their mother's growth rate. Under that assumption, the PBE given in Eq. (2) becomes

$$\frac{\partial X(\mu,t)}{\partial t} = -\frac{\partial}{\partial \mu}(X(\mu,t)\zeta(\mu)) + \mu X(\mu,t) \tag{3}$$

The first term on the right hand side of Eq. (3) is the net flux of biomass moving in μ-space. ζ represents the velocity in that space.

The model actually distinguishes an upward velocity, ζ^u computed using a time constant T^u characterizing the upward adaptation, and a downward velocity ζ^d computed with a similar time constant T^d.

$$\zeta^u(\mu) \approx \left(T^{u-1} + \mu\right)(\mu^* - \mu) \tag{4}$$

$$\zeta^d(\mu) \approx \left(T^{d-1} + \mu\right)(\mu^* - \mu) \tag{5}$$

This formulation implies that the population will tend to reach a balanced growth rate μ^* representing the optimal growth rate considering local concentrations. We can assume that the relationship between μ^* and those local concentrations is known.

In order to solve this PBE, we use a discretization method. Previous equations have then been discretized and their exact formulations are given in previous work (Morchain et al., 2013). The biological population is segregated within J classes referred by $j \in \{1, \ldots, J\}$. Each class is characterized by its biological growth rate μ_j:

$$\mu_j = \mu_{\max}\frac{j-1}{J-1} \tag{6}$$

The biomass concentration within the class j is noted X_j, the total biomass concentration X_T is then given by

$$X_T = \sum_{j=1}^{J} X_j \tag{7}$$

Each concentration X_j is transported by the liquid phase as dissolved species, which allow applying Eq. (1) to those J concentrations.

The migration of biomass between classes is presented in Fig. 2. A change in the environment results in a modification of the optimal growth rate, μ^*, represented by the double-arrow in Fig. 2. The population does not adapt immediately to the new environment, but migrates toward the two classes surrounding μ^* at a rate controlled by the time constants T^u and T^d.

The second term of Eq. (3) represents the formation of new cells with a growth rate equal to μ. After discretizing this term, we introduce the actual growth rate μ_j^a. Indeed, if the environmental conditions are favorable, cells will be able to achieve the growth rate μ_j corresponding to their class. If the environment is limiting, cells will not be able to grow at their potential growth rate μ_j and will be limited to the maximum growth rate possible in that environment, μ^*. Thus, the actual growth rate in each class is calculated as the minimum of the two: $\mu_j^a = \min\left(\mu_j, \mu^*\right)$. In the discretized

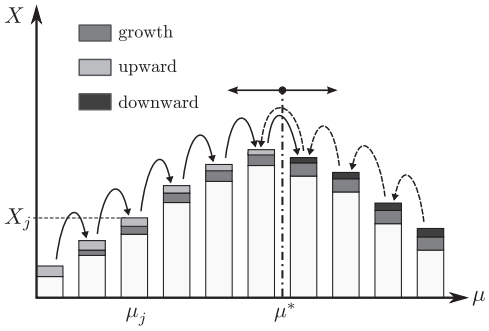

Fig. 2. Schematic representation of mechanisms affecting the specific growth rate distribution.

version of Eq. (3), the rate of cell production is therefore defined as $\mu_j^a X_j$. See also Appendix A for further details.

It is noteworthy that cells with a specific growth rate smaller than μ^* are limited by their own biological capabilities whereas those having a specific growth rate higher than μ^* will be limited by the environment. Although the environment is the same for all cells, their metabolic behaviors are therefore expected to be different. The population balance model thus introduces inertia, or time delay, in the dynamic response of the cell population to a changing environment. It decouples the actual growth rate of the population from local concentrations.

2.3. Metabolic model

2.3.1. General description

The metabolic model is invoked for each class of individuals described in the population balance model. It allows the calculation of the specific reaction rates for each group of individuals. This step only requires the knowledge of the concentrations in the liquid phase and the specific growth rate of individuals (related to their class index).

Our metabolic model for *E. coli* is based on the one described by Xu et al. (1999): their model details the growth of *E. coli* in aerobic conditions in the presence of glucose or acetate. They considered a metabolism, called “overflow metabolism”, leading to acetate formation when the oxidative pathway for energy production was saturated.

Based on their work, we added a fermentative pathway for energy production triggered in anaerobic conditions, or when the oxidative pathway is saturated. We also dissociated the overflow metabolism from energy or biomass production, which was not the case in Xu et al.'s model. Now, this metabolism is triggered when there is a disequilibrium between glucose assimilation and needs. Finally, we used the Pirt's formulation (Pirt, 1965) to estimate the conversion yield of glucose in biomass as explained in Appendix A.

Then, our metabolic model is based on four categories of biological reactions:

- Anabolism (*ana*): biomass production through glucose (or acetate) and energy consumption.
- Oxidative catabolism (*oxy*): energy production through oxidative pathway.
- Fermentative catabolism (*ferm*): energy production through fermentative pathway (mixed-acid fermentation).
- Metabolism (*over*): production of acetate through glucose overconsumption.

The oxidative and fermentative catabolism pathways allow to produce the energy needed for biomass growth. In presence of oxygen, the oxidative pathway will be preferably used for its better energetic yield. The fermentative pathway is triggered only when

the energetic need for growth is not fulfilled by the oxidative pathway, it leads to acetate formation.

It is known that *E. coli* is able to grow using glucose (G), or acetate (A) if glucose is depleted, as carbon source. If a cell consumes more glucose than what it is able to use, the amount in excess will be converted in acetate through the overflow metabolism (Matsuoka and Shimizu, 2013). In our work, we assimilated the energy to molecules of Adenosine TriPhosphate (ATP, noted E) which is the main energy source used for cellular functions.

Those considerations lead to the following set of reactions, represented in Fig. 3:

$$G + Y_{EG}E \xrightarrow{q^G_{ana}} Y_{XG}X \tag{R1}$$

$$A + Y_{EA}E \xrightarrow{q^A_{ana}} Y_{XA}X \tag{R1′}$$

$$G + Y_{OG}O \xrightarrow{q^G_{oxy}} Y^o_{EG}E \tag{R2}$$

$$A + Y_{OA}O \xrightarrow{q^A_{oxy}} Y^o_{EA}E \tag{R2′}$$

$$G \xrightarrow{q^G_{ferm}} Y^f_{EG}E + Y_{AG}A \tag{R3}$$

$$G \xrightarrow{q^G_{over}} Y_{AG}A \tag{R4}$$

With Y_{BA} being stoichiometric molar coefficients in $\mathrm{mol}_B\ \mathrm{mol}_A^{-1}$ while q^G_α and q^A_α are the specific reaction rates on G and A respectively expressed in $\mathrm{mol}_G\ g_X^{-1}\ \mathrm{h}^{-1}$ and $mol_A\ g_X^{-1}\ \mathrm{h}^{-1}$.

2.3.2. Solution procedure

The improvements made between Xu et al.'s model and ours do not rely only on the new fermentative reaction, but mainly on its strong coupling with the population balance model. Our goal is here to estimate the reaction rates for individuals in each class. When solving the ODEs set, the following procedure will be called for each class of the population balance model in each compartment of the hydrodynamic model. Although modern metabolic flux calculations now refer to time-consuming optimization methods, our procedure is a hierarchic method, consisting in a set of tests, similar to the method used by Xu et al. (1999). The advantage of the simple method adopted here is to allow a direct and rapid calculation of the reaction rates.

First, let us dissociate the overflow reaction (R_4) from "useful reactions". By useful reaction, we mean the reactions whose goal is the production of new cells, through direct production (anabolism: R_1 and R_1') or energy production (catabolism: R_2, R_2' and R_3).

Our main hypothesis is that there is an energetic balance within a cell: the rate of ATP production through catabolism reactions must be equal to the rate of ATP consumption by anabolism. Under that assumption, we will be able to define a method to estimate the useful reaction rates of a cell, just by knowing its specific growth rate μ_j, and liquid-phase concentrations (G, A, O). This method is represented by the hereunder function f, and is detailed in Appendix A.

$$f : [0,\ \mu_{\max}] \times \mathbb{R}^3_+ \longrightarrow \mathbb{R}^5 (\mu_j, G, A, O) \mapsto (q^G_{ana}, q^A_{ana}, q^G_{oxy}, q^A_{oxy}, q^G_{ferm}) \tag{8}$$

With this method defined, the overflow reaction rate is the only one missing. In our model, this metabolism is triggered when a cell consumes (or uptakes) more glucose than what is needed for its growth.

Let us note ~~that~~ Φ^u_G the useful glucose uptake rate, i.e. the amount of glucose which is used by anabolism and catabolism reactions. This rate is then defined as

$$\Phi^u_{G,j} = q^G_{ana,j} + q^G_{oxy,j} + q^G_{ferm,j} \tag{9}$$

The reaction rate of the overflow metabolism, will simply be the difference between the total glucose uptake rate $\Phi_{G,j}$ and the useful part of this rate $\Phi^u_{G,j}$:

$$q^G_{over,j} = \Phi_{G,j} - \Phi^u_{G,j} \tag{10}$$

Closing this problem finally requires an estimation of the total glucose uptake rate $\Phi_{G,j}$. It has been observed that the glucose uptake rate, in continuous cultures of *E. coli*, is not correlated to the growth rate (Leegwater et al., 1982; Natarajan and Srienc, 2000). In other words, the glucose uptake rate will be the same for all cells, no matter their class-index.

As cells dynamically adapt their uptake capacity in response to substrate fluctuations (Ferenci, 1996), our proposal is to consider that the regulation of the uptake system is fast compared to the characteristic time of concentration fluctuations. This adaptation of the uptake system will be made in order to uptake the amount of glucose that would be needed for internal reactions if the cell were at equilibrium with the environment.

By definition, cells at equilibrium do not produce overflow metabolites and therefore $\Phi_{G,j}$ can be expressed as

$$\forall j \in \{1, \ldots, J\}, \Phi_{G,j} = \Phi^*_G = \Phi^u_G(\mu^*) \tag{11}$$

In other words, the glucose uptake rate equals the sum of glucose internal utilization rates of a cell whose biological growth rate is $\mu_j = \mu^*$.

The last requirement in this procedure is an expression for μ^*. This equilibrium growth rate represents the mean growth rate of a biological population adapted to its environment. Usually, this

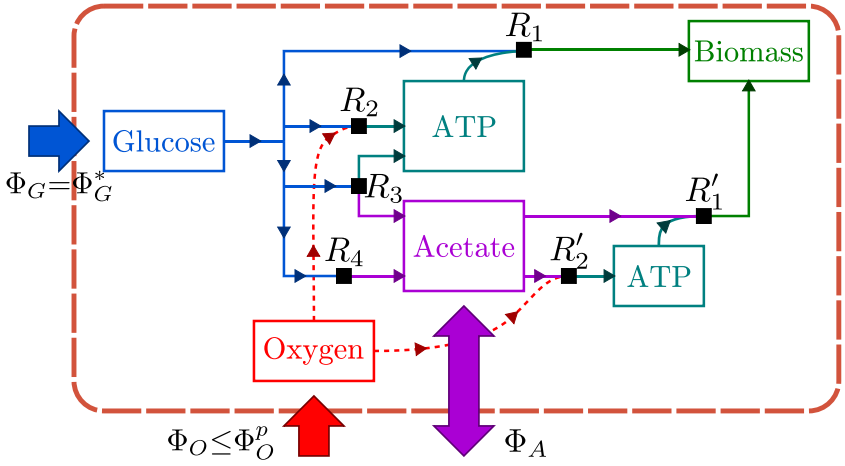

Fig. 3. Representation of the internal reactions considered in the metabolic model.

growth rate is modelized using an empirical law such as a Monod formulation which we used here.

We consider growth on two different substrates: glucose and acetate. The presence of glucose strongly inhibits the use of acetate (Xu et al., 1999). Moreover, acetate is known for its inhibition properties. This leads to the following formulation for μ^* :

$$\mu^{G*} = \mu^G_{max} \frac{G}{G+K_G} \frac{O}{O+K_O} \frac{K_{i,A}}{A+K_{i,A}} \tag{12}$$

$$\mu^{A*} = \mu^A_{max} \frac{A}{A+K_A} \frac{O}{O+K_O} \frac{K_{i,G}}{G+K_{i,G}.} \tag{13}$$

$$\mu^* = \mu^{G*} + \mu^{A*} \tag{14}$$

Summing up, the calculation process requires the following steps:

(i) Estimate the equilibrium growth rate from local concentrations:

$G, A, O \mapsto \mu^*$

(ii) Estimate the glucose consumption rate of a virtual cell at equilibrium with its environment:

$(q^{G*}_\alpha, q^{A*}_\alpha) = f(\mu^*, G, A, O)$, α stands for any reaction (anabolism, catabolism, etc.)

(iii) Deduce the population glucose uptake rate from this balanced state:

$\Phi_G = \Phi^u_G(\mu^*) = q^{G*}_{ana} + q^{G*}_{oxy} + q^{G*}_{ferm}$

(iv) In each class $j \in \{1, \ldots, J\}$, estimate the internal reaction rates for anabolism and catabolism:

$(q^G_{\alpha,j}, q^A_{\alpha,j}) = f(\mu_j, G, A, O)$

(v) In each class, deduce from precedent results the overflow reaction rate:

$q^G_{over,j} = \Phi_G - q^G_{ana,j} - q^G_{oxy,j} - q^G_{ferm,j}$

It must be understood that all these reaction rates will strongly depend on the class-index of the considered cell. In the same environment, two cells of different classes will exhibit very different behaviors. An illustration of the variety of behaviors encountered in a same population, for a particular environment, is given in Appendix A after the presentation of the method *f*.

2.3.3. Overall reaction rates

Knowing the reaction rates for each reaction, the specific consumption or production rates $r_{i,j}$ in $g_i\, g_{X_j}^{-1}\, h^{-1}$ are calculated:

$$r_{X,j} = \left(q^G_{ana,j} Y_{XG} + q^A_{ana,j} Y_{XA}\right) M_X = \mu^a_j \tag{15}$$

$$r_{G,j} = -\left(q^G_{ana,j} + q^G_{oxy,j} + q^G_{ferm,j} + q^G_{over,j}\right) M_G \tag{16}$$

$$r_{A,j} = \left(q^G_{ferm,j} Y_{AG} + q^G_{over,j} Y_{AG} - q^A_{oxy,j} - q^A_{ana,j}\right) M_A \tag{17}$$

$$r_{O,j} = -\left(q^G_{oxy,j} Y_{OG} + q^A_{oxy,j} Y_{OA}\right) M_O \tag{18}$$

The volumetric reaction rates needed in the mass conservation equation (Eq. (1)), R_i in $g_i\, L^{-1}\, h^{-1}$ with $i \in \{X, G, A, O\}$, are easily obtained from a summation of the specific rates over the entire population:

$$R_i = \sum_{j=1}^{J} r_{i,j} X_j \tag{19}$$

For all specific variables, i.e. variables expressed per gram of biomass (subscript *j*), we define a mean variable over the population using the notation $\tilde{}$. Thus, the population growth rate, noted $\tilde{\mu^a}$, is given by

$$\tilde{\mu^a} = \frac{1}{X_T} \sum_{j=1}^{J} (\mu^a_j X_j) \tag{20}$$

Note that $\tilde{\mu^a}$ is the growth rate experimentally observed.

Model parameters used in our simulations of *E. coli* cultivations are given in Tables 1 and 2.

3. Results

3.1. Batch culture

First, our biological model has been challenged by a set of experimental data coming from a batch culture conducted in a 15 liters stirred tank reactor. This culture and related measurement methods have been described by Xu et al. (1999). From these data, it can be assumed that mixing and oxygen mass transfer were not limiting, so that the reactor is treated as perfectly mixed. Thus, the associated Compartment Model consisted in a single compartment ($M^f = 0$). In the experiment, the oxygen concentration was regulated around a value corresponding to 30% of saturation. Accordingly it was decided to discard the conservation equation for oxygen in the liquid phase and to impose a constant value in the simulations.

During a 12 h culture, measurements of glucose, biomass and acetate concentrations were carried out each hour. Plus, a respirometric monitoring allowed to determine the Oxygen Consumption Rate (*OCR* in $mmol_O\, L^{-1}\, h^{-1}$). In that paper the authors proposed a metabolic model for aerobic cultivation of *E. coli* in which overflow metabolism resulted from the saturation of the oxidative capacity of cells. Our formulation is slightly different: overflow results from an extra assimilation of substrate compared to the cell needs. The latter may include energy production by fermentation if the oxidative capacity is saturated. Therefore it was essential to check

Table 1
Model constants for *E. coli*.

Symbol	Value	Unit	Source
Molar masses			
M_X	113.1	$g_X\, mol_X^{-1}$	[a]
M_G	180.2	$g_G\, mol_G^{-1}$	
M_O	32.0	$g_O\, mol_O^{-1}$	
M_A	59.0	$g_A\, mol_A^{-1}$	
Affinity and inhibition constants			
K_G	0.05	$g_G\, L^{-1}$	0.05[b] 0.095[c]
K_A	0.05	$g_A\, L^{-1}$	0.05[b]
K_O	0.1	$mg_O\, L^{-1}$	0.0768[c] 0.1[d]
$K_{i,G}$	0.2	$g_G\, L^{-1}$	
$K_{i,A}$	3.0[e]	$g_A\, L^{-1}$	4.0–5.0[b]
$K^o_{i,A}$	4.0	$g_A\, L^{-1}$	4.0[b]

[a] The biomass is represented by the typical chemical formula $C_5H_7NO_2$.
[b] Xu et al. (1999).
[c] Meadows et al. (2010).
[d] Morchain et al. (2013).
[e] Curve fitting.

Table 2
Model constants for *E. coli*

Symbol	Value	Unit	Source
Molar yields			
Y_{EG}	12.05	$mol_E\ mol_G^{-1}$	
Y_{XG}^{max}	1.32	$mol_X\ mol_G^{-1}$	$1.25_{\pm 0.05}$[a]
m	250	$\mu mol_G\ g_X^{-1}.h^{-1}$	310[b]; 220[c]; $350_{\pm 40}$[d]
Y_{OG}	6.0	$mol_O\ mol_G^{-1}$	6.0[c,d]
Y_{EG}^{o}	20.0	$mol_E\ mol_G^{-1}$	18.7[d]
Y_{EG}^{f}	3.0	$mol_E\ mol_G^{-1}$	3.0[e]
Y_{AG}	2.0	$mol_A\ mol_G^{-1}$	2.0[c]
Y_{EA}	4.0	$mol_E\ mol_A^{-1}$	
Y_{XA}	0.40[f]	$mol_X\ mol_A^{-1}$	0.21[c]
Y_{OA}	2.0	$mol_O\ mol_A^{-1}$	2.0[c,d]
Y_{EA}^{o}	4.67	$mol_E\ mol_A^{-1}$	4.67[d]
Biological limitations			
μ_{max}^{G}	0.663	$g_X.g_X^{-1}\ h^{-1}$	$0.676_{\pm 0.038}$[g]
μ_{max}^{A}	0.032	$g_X\ g_X^{-1}\ h^{-1}$	$0.052_{\pm 0.028}$[g]
Φ_O^{max}	15.6	$mmol_O\ g_X^{-1}\ h^{-1}$	$15.3_{\pm 19}$[e]; 20[d,h]
Growth rate adaptation			
T^u	1.9	h	1.9[i]
T^d	6.7[f]	h	1.9[i]

[a] Values extracted from Xu's overall yield $Y_{X/S,of}$ and $Y_{X/S,ov}$ (Xu et al., 1999) coupled with our $Y_{EG}^{\varnothing/f/o}$ values.
[b] Russell and Cook (1995).
[c] Xu et al. (1999).
[d] Varma et al. (1993).
[e] Wang et al. (2010).
[f] Curve fitting.
[g] Extracted from Xu's $qA_{c,max}$, qS_{max}, $Y_{X/A}$ and $Y_{X/S,ox}$ (Xu et al., 1999).
[h] Meadows et al. (2010).
[i] Morchain and Fonade (2009).

that our modification constitutes a real improvement while preserving the original model capacities.

Results for batch culture simulations with both models, as well as experimental data, are shown in Fig. 4a,b,e,f. The initial concentrations used for simulations are detailed in Table 3. The initial biomass concentration, X_0, was not reported by Xu et al. (1999). After implementing the original model described by these authors, the initial biomass concentration could be identified through a curve fitting of the data. The value obtained was also used as the initial condition for our simulations.

We decided to initialize the population in the class corresponding to $\mu_j = 0.4\ h^{-1}$. This value is chosen as it gives the best fitting of experimental data. The reason for this choice is further detailed at the beginning of the discussion section.

The results presented in Fig. 4 were obtained using 100 classes in our population balance model. Unpublished data show that the simulation results are independent from the number of classes as long as this number is higher than 60.

Fig. 4a and b represents the concentrations of glucose and acetate over time. The substrate consumption is perfectly represented by both models, however those models differ in the way this substrate is used, leading to a difference in acetate production. When glucose is depleted, the acetate is re-consumed at a rate consistent with experimental observation. Our model provides a much better fit of the experimental data which is not the result of a parameter adjustment as will be discussed later on. Fig. 4e and f shows a good prediction of oxygen consumption as long as glucose is present. This prediction becomes less accurate as soon as this substrate is entirely consumed. In such a situation, some phenomena like endogenous metabolisms are known to participate in the oxygen consumption. Yet, such details are not implemented in our model, leading to those prediction errors.

The experimental concentrations have been post-processed to determine the experimental apparent growth rate $\tilde{\mu^a}$ and acetate variation rate $\tilde{r_A}$ as detailed in the following equations:

$$\tilde{\mu^a}\left(\frac{t_i+t_{i+1}}{2}\right) = \frac{X_{i+1}-X_i}{t_{i+1}-t_i}\left(\frac{X_i+X_{i+1}}{2}\right)^{-1} \quad (21)$$

$$\tilde{r_A}\left(\frac{t_i+t_{i+1}}{2}\right) = \frac{A_{i+1}-A_i}{t_{i+1}-t_i}\left(\frac{X_i+X_{i+1}}{2}\right)^{-1} \quad (22)$$

With A and X being the experimental concentrations of Acetate (in $g_A\ L^{-1}$) and Biomass (in $g_X\ L^{-1}$). The subscripts i and $i+1$ refer to two consecutive samples and analysis.

As shown in Fig. 4b, our model predicts acetate formation almost perfectly compared to Xu et al's model. This is mainly explained by the way our model differentiates the two acetate origins: the fermentation, and the overflow metabolism.

At initial conditions, glucose and oxygen concentrations are high compared to their affinity constants, meaning that culture conditions are optimal (here, $\mu_0^* \approx 0.64\ h^{-1}$). Meanwhile, it is observed experimentally that the specific rate of acetate production is high too. However, Xu et al.'s model is not able to predict that high initial acetate production (Fig. 4d): only a constant production rate is predicted, and is correlated to an oxygen deficiency caused by a low value of the maximum oxygen uptake rate. On the opposite, our own model differentiate two phases in the acetate production. In our model the glucose uptake rate is correlated to μ^*, which happens to be high initially. However, we initialized the biological population in a unique class such as $\tilde{\mu} = 0.4\ h^{-1}$. Then, for the first 2 h of the culture, a disequilibrium exists between the population and its environment ($\tilde{\mu} < \mu^*$) leading to acetate formation through the overflow metabolism (see $\tilde{r}_{Aover}$ in Fig. 5b). This production decreases along with the progressive adaptation of the population to the environment.

Around 2 h, a switch between the two acetate origins occurs: the high value of $\tilde{\mu^a}$ leads to high energetic needs, saturating the oxidative catabolism pathway. Then, a fraction of the energy is produced through fermentation.

It may be observed that the curve of acetate produced by the fermentation pathway (A_{ferm} in Fig. 5a) looks alike the curve of acetate predicted by Xu et al.'s model (Fig. 4b). This tends to show that the so-called overflow metabolism used in their model consists in a fermentative metabolism. Indeed, their model links acetate production with energy and cell production as does our fermentation reaction (R_3).

Here, we chose to initialize the population with a Dirac distribution by concentrating all biomass in a unique class. However, many other distributions could have led to similar results such as, maybe, a Gaussian distribution centered around $\mu = 0.45\ h^{-1}$ or even a multimodal distribution. Here, we want to point out that there is a lack of experimental data about the state of the population in the inoculum used in biological cultures. As measurements are usually carried out at the population scale, hardly no data exists about the distribution of biological parameters even though such data appear more and more mandatory for the good comprehension of biological behaviors observed in bio-reactors (Dhar and McKinney, 2007).

The inhibition of respiration by acetate is underlined in Fig. 4e as the specific oxygen consumption rate $\tilde{\Phi_O}$ decreases significantly between 2 and 8 h. This inhibition strengthens the acetate production through fermentation by limiting the use of the oxidative pathway.

Those results allow to validate our biological model in a reactor in which hydrodynamics has no visible effect on the biological

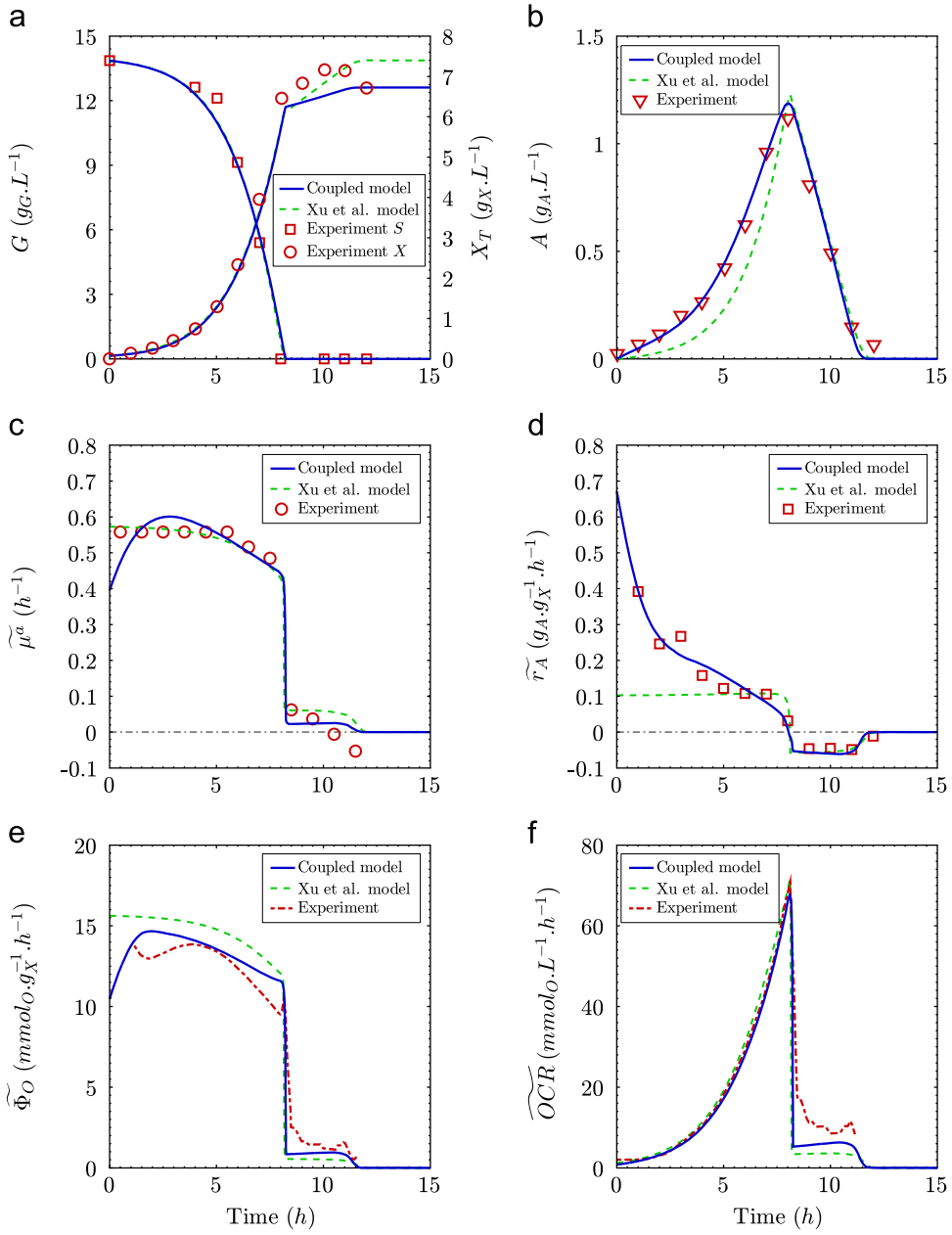

Fig. 4. Comparison of experimental data with simulation results in a batch reactor.

Table 3
Initial concentrations for batch culture.

Symbol	Value	Unit
X_0	0.077	$g_X\,L^{-1}$
A_0	0.00	$g_A\,L^{-1}$
G_0	13.86	$g_G\,L^{-1}$
O_0	2.70	$mg_O\,L^{-1}$

population. However, in large bioreactors, heterogeneities may appear under certain conditions depending on the quality of mixing and the intensity of biological reactions. Thus, the ability of our model to predict the complex transition between homogeneous and heterogeneous concentration fields has to be challenged against experimental data.

3.2. Fedbatch culture

The validation of our model in large bioreactors was performed using data provided by Xu et al. (1999a) on a fed-batch culture conducted in a 30 m^3 reactor stirred with four impellers (Rushton turbines). This reactor has been described previously (Xu et al., 1999a; Larsson et al., 1996) and its matrix of volume flow rates, M^f, was computed using the compartment model proposed by Vrábel et al. (1999, 2000, 2001) with 70 compartments. The Appendix B details the calculation of M^f for this reactor.

The validation of our implementation of this compartment model was performed through the simulation of a tracer pulse-response. Fig. 6 details the predicted relative concentration of the tracer on top, middle and bottom positions of the reactor by injecting the tracer in the top-stirrer compartment. These curves are very similar to those presented by Vrábel et al. (1999) which validates our implementation of the flow map at the reactor scale.

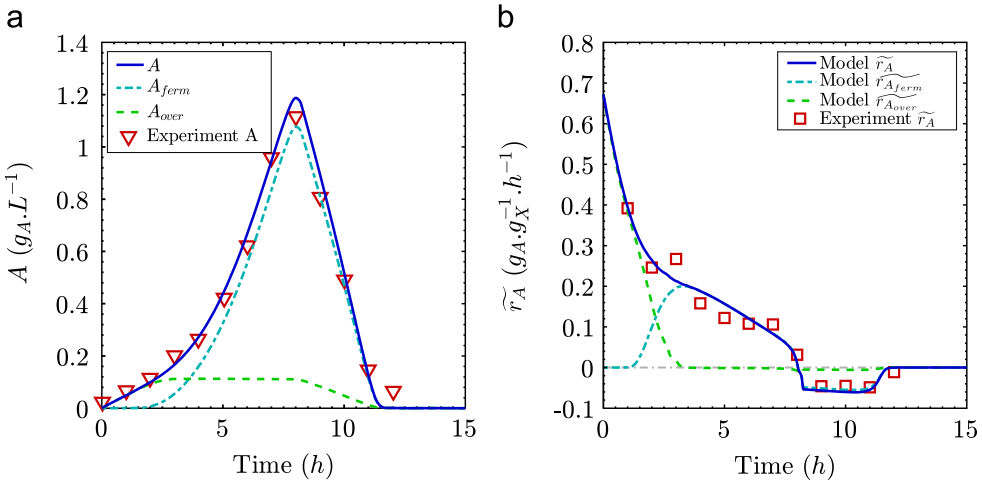

Fig. 5. Differentiation of acetate production pathway throughout the culture. A_{ferm}: acetate produced through fermentative catabolism, A_{over}: acetate produced by overflow metabolism.

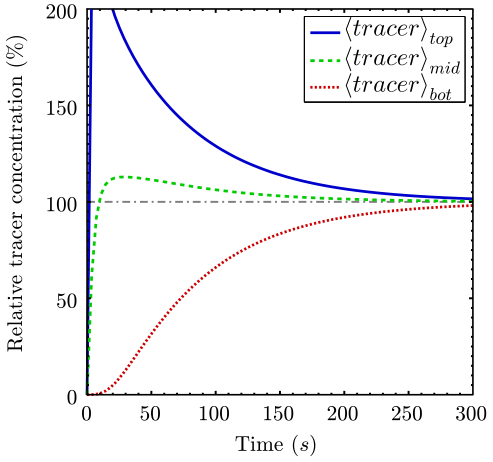

Fig. 6. Pulse-response monitoring after tracer injection in the feeding compartment.

We also deduce from this tracer experiment that the overall mixing time in this reactor is about $t_{mix} \approx 250$ s.

In the following, the notation $\langle\rangle$ describes the volumetric average of variables. By default, the volumetric average is taken over the entire reactor volume, but a subscript may be used to specify a sub-part of the reactor (top, middle or bottom). The Fig. 7 compares the results from our simulation, the experimental data (Xu et al., 1999a) and the curves coming from Xu et al.'s simulations using Xu et al.'s model (Vrábel et al., 2001). Initial conditions are reported in Table 4. The biomass was initially put in the class corresponding to $\mu_j = 0.63\ h^{-1}$ as this choice leads to the best curve fitting. As for the batch culture, consequences of this choice are detailed at the beginning of the discussion.

It is important to note that the simulation of the fedbatch culture was carried out without further adjustments of our model parameters compared to the batch culture simulation.

Fig. 7a details the evolution of glucose concentrations on top, middle and bottom positions. It should be noticed that the way Vrábel et al. (2001) modeled the feed leads to an overestimation of glucose concentration during the first hours of culture (Fig. 7a) which is not consistent with experimental measurements. Nevertheless, the same sudden shift of the feed flow rate at $t = 0.8$ h was imposed in our simulation in order to allow the assessment of the results. Both models give very similar results regarding the glucose

Table 4
Fed-batch culture—initial conditions.

	Value	Unit
Volume V_0	22	m^3
Biomass X_0	0.10	$g_X\ L^{-1}$
Glucose G_0	0.029	$g_G\ L^{-1}$
Acetate A_0	0.05	$g_A\ L^{-1}$

concentration. It is likely that a modification of the affinity constant for glucose could produce better agreement between the experimental data and the simulation results. However this does not constitute an objective for this work which is more focused on the minimal structure of a two-way coupling approach for the simulation of heterogeneous bioreactors. It will appear clearly in the next paragraphs that the benefits of the coupled approach is more related to the structure of the model than to the accuracy of the parameter identification procedure.

The first observation of interest is on the total biomass concentration $\langle X_T \rangle$ given in Fig. 7b. The mixing-time, $t_{mix} \approx 250$ s, is negligible compared to the characteristic time of biological growth (Morchain et al., 2014), then the total biomass concentration is independent of the position within the reactor. Vrábel et al.'s simulation over-predicted the biomass production and an unjustified adjustment of the conversion yield Y_{XG} by a factor as large as 0.76 was necessary to fit experimental data. Meanwhile, our model correctly predicts this production by taking into account the known phenomena of yield decrease at low growth rate using the Pirt's formulation (Pirt, 1965) as explained in Appendix A.

The next remarkable point is related to the acetate production. The acetate concentration is presented in Fig. 7c and its specific variation rate is given in Fig. 7d. In that case a noticeable difference between the model predictions appears. Whereas the model of Xu et al. predicted no residual acetate, our coupled model qualitatively predicts the transient accumulation before 10 h and the formation of a spatial gradient as the biomass concentration increases.

As shown in Fig. 7d, the acetate is produced everywhere in the reactor before 7 h. After that, it appears that acetate is produced in the upper part of the reactor and is consumed in the lower part of the reactor where the glucose concentration is very low. Moreover the data in Fig. 7d also allow the identification of the mechanisms involved. The thick dotted-dashed line corresponds to the

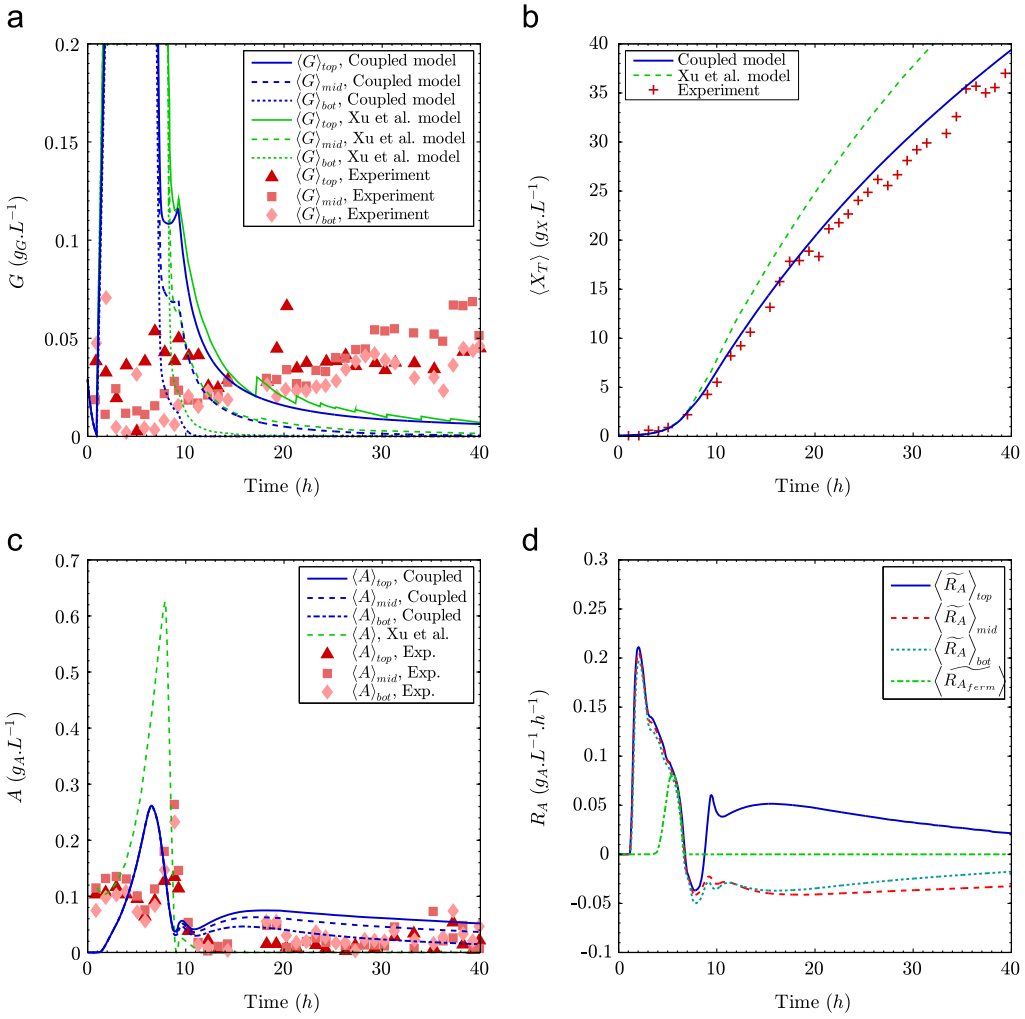

Fig. 7. Experimental data and simulation results in the 30 m^3 fedbatch reactor.

production through fermentation. The fermentation metabolism is only triggered between 4 and 7 h leading to the acetate peak observable at the same time in Fig. 7c. This demonstrates that, apart from that period of time, acetate is produced through overflow metabolism.

4. Discussion

Our modeling approach, based on population balance model, is clearly dependent on the initial conditions, obviously X and G concentrations, but also the initial growth rate distribution whose choice may have a real impact on the simulation results. This is a common feature of biological systems which has been discarded in most previous modeling approaches. From that initial distribution will depend the global kinetic of the culture, but also the initial disequilibrium between the population and its environment which leads to different metabolic behaviors.

In batch and fedbatch cultures, we decided to concentrate all the biological population in one class. The choice of that class was made in order to fit the results with experimental data.

For the batch culture, the initial population growth rate imposed in the simulation ($\mu_j = 0.4\ \mathrm{h}^{-1}$) is different from the experimental one reported by Xu et al. (1999). Based on their experimental measurements, Xu et al. (1999) estimated the initial growth rate around $\mu = 0.56\ \mathrm{h}^{-1}$. However, since initial biomass concentrations are negligible, this estimation of the initial growth rate may be flawed and we estimate, by an error analysis, that the actual growth rate is lies between $0.3\ \mathrm{h}^{-1}$ and $0.8\ \mathrm{h}^{-1}$.

With our model, the choice of the initial distribution has two main consequences: the first one is about the initial disequilibrium between the biological population and the environment. Actually, the value of μ returned by Xu et al.'s model is very similar to what we call the equilibrium growth rate, μ^*. Then, by initializing the entire population at $\mu_j = 0.4\ \mathrm{h}^{-1}$, we artificially create the initial disequilibrium that explains, with our model, the high value of $\tilde{r_A}$. Many different initial distributions could produce similar results in terms of $\tilde{r_A}$. The fact is that the experimental information on the actual distribution of growth rate at $t=0$ is not available.

The second consequence is about the global kinetic of the culture. If we initialized the biomass at $\mu_j = 0.2\ \mathrm{h}^{-1}$, we would have increased the disequilibrium, leading to an higher production of acetate, but we also would have add a lag in the biomass growth (glucose consumption would have been slower). We choose the value of $\mu_j = 0.4\ \mathrm{h}^{-1}$ as it was the best compromise between the global kinetic and the acetate production.

The same comment applies to the initial distribution of fedbatch culture. Moreover, in continuous culture (e.g. fedbatch or chemostat), the medium is continuously renewed and the duration of the culture exceeds the time scale of biological growth-rate adaptation. Then, after

a few hours, the population tends to "forget" its initial state. For example, in our fedbatch simulation, the choice of the initial distribution only has an effect for the first hours of the simulation: it is found that the initial conditions are forgotten when the culture enters the "mixing/reaction competition zone" after 7 h. So it has no fundamental impact on the observations made when the reactor becomes spatially heterogeneous.

On the results of the models, the main difference between ours and Xu et al.'s one is shown on fedbatch acetate curves. Indeed, their model was not able to predict the acetate residual concentration that is experimentally observed after 10 h of fedbatch culture while ours predicts the apparition of an acetate gradient over the reactor.

To understand this capability of our model, one must distinguish two different phases in the culture. For the 7 first hours of culture, the reactor appears homogeneous while, after 10 h, vertical gradients appear for glucose and acetate. It is worth investigating more specifically what happens during the transitional phase between 7 h and 10 h. This can be done through the time scale analysis of the various processes involved.

In a previous paper (Morchain et al., 2014), we introduced the time scale of the substrate assimilation, t_S:

$$t_G = \frac{\langle G \rangle}{\langle R_G \rangle} \approx \frac{M_X Y_{XG} \langle G \rangle}{M_G \mu_{max} \langle X_T \rangle} \tag{23}$$

Fig. 8 shows the evolution of this assimilation time-scale compared to the mixing time. It can be seen that a switch occurs around 7 h with the assimilation time becoming smaller than the mixing time. This means that at the beginning of the culture, the glucose poured into the reactor is quickly mixed compared to the reaction rate, leading to an homogeneous reactor. Then a regime switch occurs, the substrate consumption gets faster (due to an increasing biomass concentration) and substrate is now consumed before reaching the bottom of the reactor, leading to the observed gradients.

A gradient on acetate concentration appears around 2 h after the glucose gradient. This delay of 2 h results from the dynamic adaptation of the population (Eq. (4)). This clearly illustrates the of dynamic responses at the reactor scale: the acetate gradient is a consequence of the biomass adaptation to the heterogeneous glucose concentration field induced by a mixing limitation.

Those different situations may be visualized and understood in Figs. 9 and 10. It is shown that around 8 h the reactor changes from a homogeneous to a heterogeneous state. After the transitional phase, glucose is mainly present around the feeding point while a major fraction of the reactor has little or no substrate as shown in Fig. 9 top. This leads to the strong spatial variation of the equilibrium growth rate (Fig. 9 bottom). In our model, the uptake rate is closely related to local concentrations whereas the utilization rate for growth is determined by the volume average concentration. This is consistent with the fact that the adaptation of uptake systems is rather fast compared to that of the growth rate. This difference in the response dynamics is thought to be responsible for the cell disequilibrium.

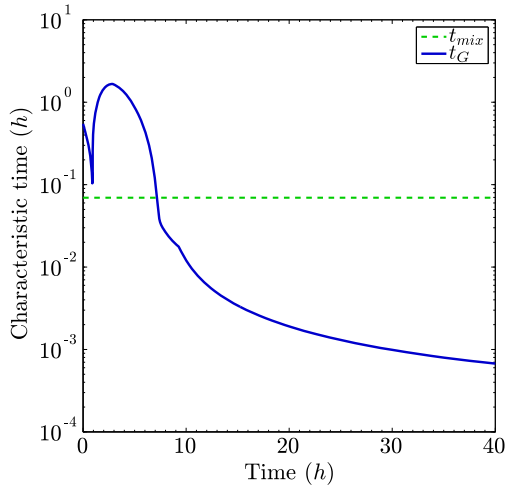

Fig. 8. Comparison of mixing and substrate assimilation time scales during the fedbatch culture.

As explained previously, the overflow metabolism is triggered when the biomass is in a rich-in-substrate environment while being adapted to a limiting environment. This is what happens during the heterogeneous phase: the biomass is accustomed to a mean concentration but happens to be in a high concentration zone around the feeding point, and in low concentration zones elsewhere, leading to a permanent disequilibrium (Fig. 10 top). This unbalanced population reacts by producing acetate through overflow in the feeding area. This acetate is afterward transported in the areas with low glucose concentrations and is consumed there by the starving biomass, leading to the acetate gradient as underlined in Fig. 10 bottom.

Furthermore, it is interesting to observe that, the time constant of growth rate adaptation being larger than the circulation time, the mean biological growth rate $\tilde{\mu}$ is related to the volume average concentration of glucose $\langle G \rangle$. Thus, as already demonstrated in a previous work, the population distribution in the μ-space is independent of the location in the reactor, but the difference between the population state and the local environment is spatially dependent (Morchain et al., 2014). Although the time constant related to the specific growth rate adaptation is much larger than the mixing time, the repeated exposure to high and low concentrations over hours has a significant effect on the width of specific growth rate distribution of the population. Indeed, Fig. 11 shows the evolution of the population distribution over classes compared with the equilibrium growth rate in different areas of the reactor. The width of the distribution is related to the width of the colored zone around the volumetric mean. In this figure β is defined by

$$\beta(t, \mu_j) = \frac{X_j(t)}{\max_{j=1}^{J}(X_j(t))} \tag{24}$$

It is indicative of the population growth rate distribution width (note that only values higher than 5% are shown). Thus it is visible that the population is always distributed (and almost centered) around the mean volumetric growth rate.

It may be seen that after 10 h, when a major volumetric fraction of this reactor has low glucose concentrations, the population gets used to these low concentrations by moving to lowest classes. Then, this population is no longer capable to use the glucose efficiently when being in the feeding area, leading to these high local acetate productions.

Such phenomena may only be predicted by considering the disequilibrium between the substrate consumption and the cell needs. The quantification of this disequilibrium relies upon the use of a population balance model to describe the dynamic adaptation of the growth rate.

In the present work, we considered in our modeling that biological heterogeneity in terms of growth rate distribution is induced by the environment (exogenous heterogeneity). In a chemostat, this characteristic of the model ensures that the population growth rate will tend, in the long term, to the dilution rate. In a constant environment, all cells will be distributed in the two classes surrounding μ^* as shown in Morchain et al. (2013). However, recent experimental data indicate that an interdivision time distribution exists in a chemostat (Nobs and Maerkl, 2014). It implies that endogenous source of heterogeneity is also present.

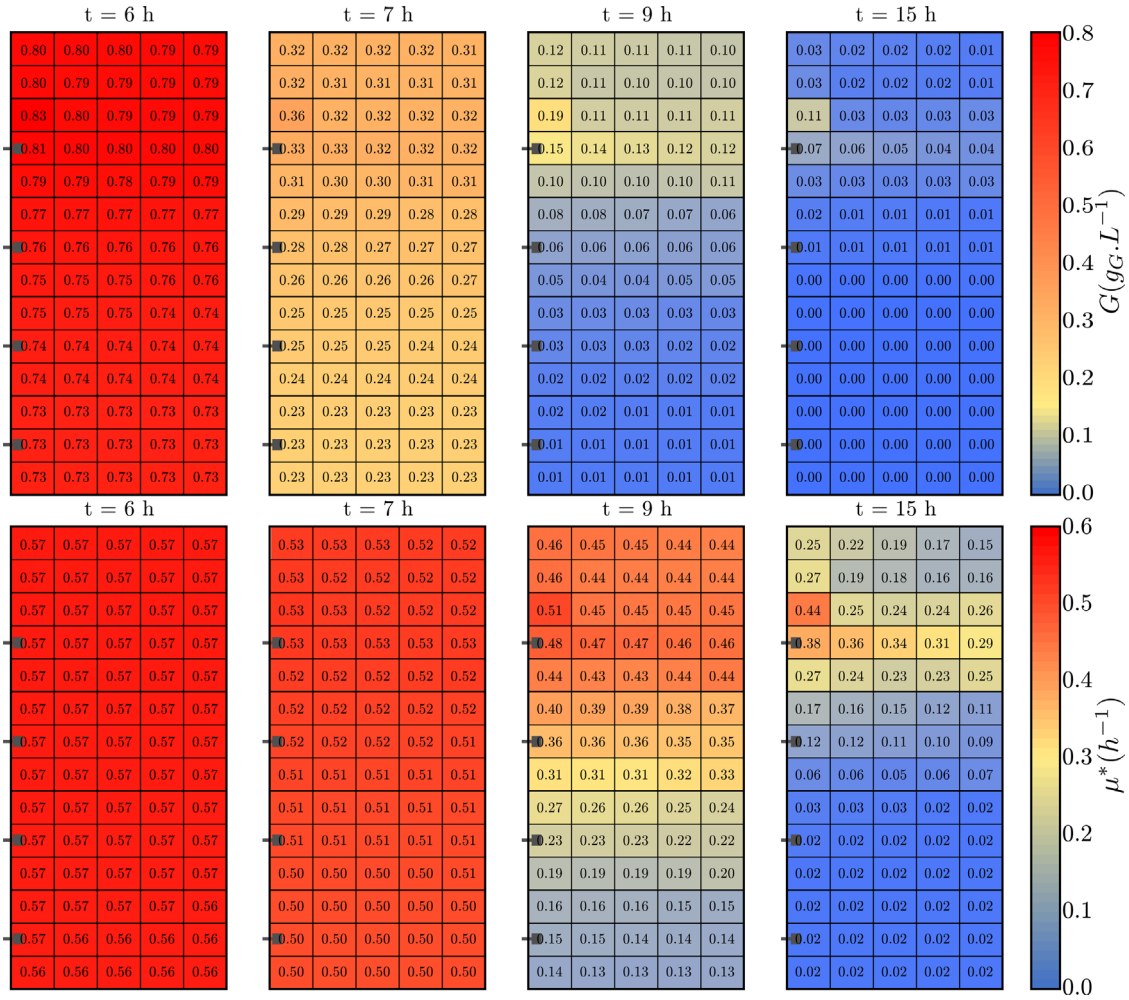

Fig. 9. Glucose concentration field (top) and related equilibrium growth rates (bottom) in the 30 m^3 reactor during the cultivation. The grid corresponds to the 70 compartments of the hydrodynamic model. The numerical data are local instantaneous values.

Taking this fact into account in the modeling constitutes a potential way for future improvements. Still, the current formulation proposed in this work remains meaningful in a large scale bioreactor in which concentration gradients are present and play a dominant role in the production of heterogeneity within the population.

5. Conclusions

In this work, we focused on the dynamic simulation of bioreactors. Due to the strong two-way coupling between the biological behavior and the spatial and temporal variations of concentration fields, we introduced a modeling using a metabolic and a population balance models. It leads to the description of a possible disequilibrium between the biomass and its environment, interpreted as an imbalance between a cell needs and its actual glucose consumption. This modelization has been applied to the well known bacteria *Escherichia coli* in order to challenge our model with data extracted from the literature.

We integrated this biological model with a compartment model describing the hydrodynamics of two reactors of different scales: (i) a 15 L homogeneous reactor and (ii) a 30 m^3 stirred reactor. Our model was consistent enough to allow good predictions of experimental measurements at two reactor scales without modifying its parameters. Thus, we shown that the coupling of a metabolic and a population balance models strongly improves the prediction of acetate production, as well as the overall biological behavior, compared to the standalone metabolic model. In particular, we observed that the formation of a glucose gradient necessarily induces the production and the consumption of acetate in different zones of the reactor. Such phenomena could not be predicted without introducing an unbalanced biomass in our modeling. So it is believed that these concepts leading to a two-way coupled approach is a promising way to address the issue of simulating industrial bioreactors.

Notation

Roman

A	acetate
E	energy, molecule of ATP
G	glucose
J	number of classes
K	affinity or inhibition biological constant ($g\,L^{-1}$)
M	molar mass ($g\,mol^{-1}$)
m	maintenance rate ($mol_G\,g_X^{-1}.h^{-1}$)
M^f	matrix of volume flow rates

N	number of compartments
O	oxygen
q	specific reaction rate (mol g_X^{-1} h^{-1})
R	volumetric reaction rate (g L^{-1} h^{-1})
r	specific reaction rate (g g_X^{-1} h^{-1})
T	volumetric transfer rate (g L^{-1} h^{-1})
T^d	time constant for downward transfer between classes (h)
T^u	time constant for upward transfer between classes (h)
t	time (h)
X	cells, biomass
Y	stoichiometric molar coefficient (mol mol^{-1})

Subscript and superscript

$*$	variable describing a cell at equilibrium with its environment
0	initial conditions
a	actual or achieved
f	fermentative reaction
i	generic notation for any species (A, E, G, O or X)
j	class index
m	compartment index
max	maximum value of a biological constant
n	compartment index
o	oxidative reaction
T	total over the biological population

Greek

α	generic notation for any biological reaction
Φ	biological uptake rate (mol g_X^{-1} h^{-1})
μ	specific growth rate of a cell (h^{-1})
ζ	rate of change of specific growth rate (h^{-2})

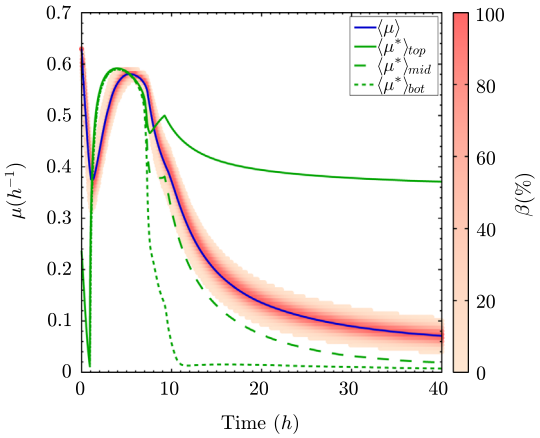

Fig. 11. Evolution of biological population width, and equilibrium growth rates at different locations in the reactor.

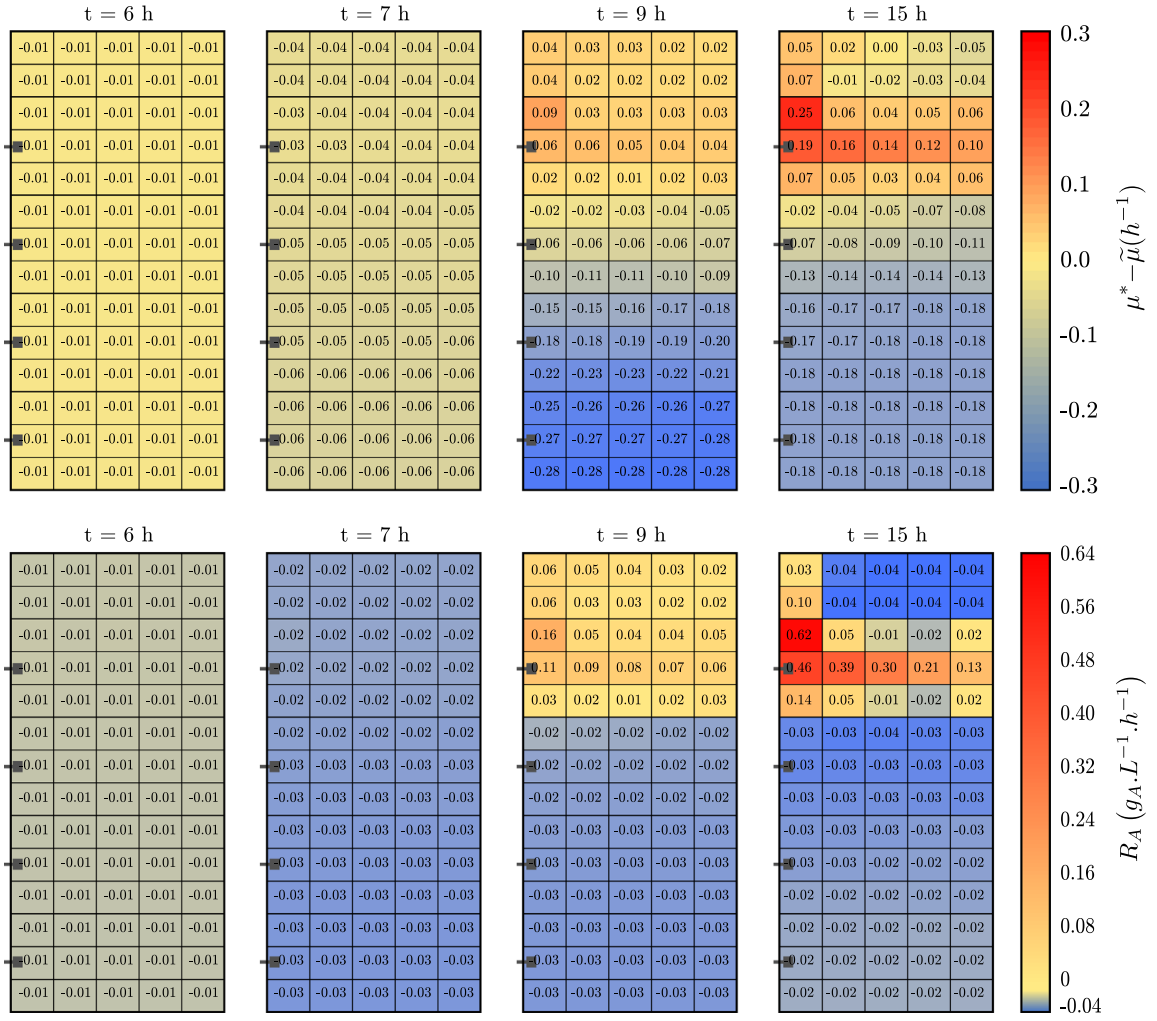

Fig. 10. Overall population disequilibrium expressed as $\mu^* - \tilde{\mu}$ (top) and acetate production/consumption rates (bottom). The grid corresponds to the 70 compartments of the hydrodynamic model. The numerical data are local instantaneous values.

Acknowledgments

The authors would like to thank Toulouse White Biotechnology UMS INRA 1337, UMS CNRS 3582 for its financial support. The authors declare no conflict of interest.

Appendix A. Metabolic reaction rates calculation

This appendix details explicitly the calculation procedure of biological reaction rates. It presents a method to calculate these reactions rates, starting from the cell biological growth rate μ_j and the liquid-phase concentrations (in glucose (G), acetate (A) and oxygen (O)). In its principle, this method is similar to that proposed by Xu et al. (1999): it consists in a set of tests (hierarchic method). This procedure defines the rates of the following reactions:

$$G + Y_{EG}E \xrightarrow{q^G_{ana}} Y_{XG}X \tag{R1}$$

$$A + Y_{EA}E \xrightarrow{q^A_{ana}} Y_{XA}X \tag{R1′}$$

$$G + Y_{OG}O \xrightarrow{q^G_{oxy}} Y^o_{EG}E \tag{R2}$$

$$A + Y_{OA}O \xrightarrow{q^A_{oxy}} Y^o_{EA}E \tag{R2′}$$

$$G \xrightarrow{q^G_{ferm}} Y^f_{EG}E + Y_{AG}A \tag{R3}$$

This estimation is here possible by assuming an energetic balance within a cell: the rate of ATP production, through catabolism pathways, is strictly equal to the rate of ATP consumption through anabolism:

$$Y^o_{EG}q^G_{oxy} + Y^f_{EG}q^G_{ferm} = Y_{EG}q^G_{ana} \tag{A.1}$$

$$Y^o_{EA}q^A_{oxy} = Y_{EA}q^A_{ana} \tag{A.2}$$

First, we must evaluate the actual growth rate of the considered cell. We consider that growth may be limited either by the biological growth rate (internal limitation), or by the environment concentrations (external limitation). Those concentrations allow to compute an environment permitted (or equilibrium) growth-rate μ^* :

$$\mu^{G*} = \mu^G_{max}\frac{G}{G+K_G}\frac{O}{O+K_O}\frac{K_{i,A}}{A+K_{i,A}} \tag{A.3}$$

$$\mu^{A*} = \mu^A_{max}\frac{A}{A+K_A}\frac{O}{O+K_O}\frac{K_{i,G}}{G+K_{i,G}} \tag{A.4}$$

$$\mu^* = \mu^{G*} + \mu^{A*} \tag{A.5}$$

Then, the actual growth rate is defined as the minimum between the biological, and the equilibrium, growth rates. We define an actual growth rate for glucose-based growth ($\mu^{a,G}_j$), and an other one for acetate-based growth ($\mu^{a,A}_j$). The sum of them leads to the actual growth rate of the cell:

$$\mu^{a,G}_j = \min\left(\mu_j, \mu^{G*}\right) \tag{A.6}$$

$$\mu^{a,A}_j = \min\left(\mu_j - \mu^{a,G}_j, \mu^{A*}\right) \tag{A.7}$$

$$\mu^a_j = \mu^{a,G}_j + \mu^{a,A}_j = \min\left(\mu_j, \mu^*\right) \tag{A.8}$$

Anabolism

The anabolism reaction rates are directly deduced from the actual growth rates, on G (Eq. (A.10)) and A (Eq. (A.11)), of the j-th class. The conversion yield of glucose in biomass, Y_{XG}, is computed using the Pirt's formulation (Pirt, 1965). This formulation, given in Eq. (A.9), reflects the fact that maintenance operations take a major role in substrate consumption at low growth rate while having a negligible effect at high growth rate (Russell and Cook, 1995):

$$\frac{1}{Y_{XG}} = \frac{m \times M_X}{\mu^a_j} + \frac{1}{Y^{max}_{XG}} \tag{A.9}$$

m (in $mol_G\, g_X^{-1}\, h^{-1}$) is the maintenance rate, representing the amount of substrate needed for maintenance. In the present work, m was kept constant at 250 $\mu mol_G\, g_X^{-1}\, h^{-1}$, but for a more detailed model it has been suggested that this rate is partially linked to the growth rate (Holms, 1996; Meadows et al., 2010).

$$q^G_{ana,j} = \frac{\mu^{a,G}_j}{Y_{XG}M_X} \tag{A.10}$$

$$q^A_{ana,j} = \frac{\mu^{a,A}_j}{Y_{XA}M_X} \tag{A.11}$$

Those rates represent a cell-production rate that will effectively be achieved. But to allow this cell production, energy must be produced as well. We then must estimate the rate of energy production through the oxidative pathway, and if needed, through the fermentative pathway.

Catabolism

As the oxidative pathway provides a better energetic yield, we make the assumption that the energy needed for anabolism will be only produced through that pathway if possible. The fermentative pathway will only be triggered if there is an oxygen deficiency.

First, lets estimate the amount of oxygen that would be needed (upper-script n) to produce all the energy needed. In that case, the oxidative catabolism reaction rates would be

$$q^{G,n}_{oxy,j} = \frac{Y_{EG}q^G_{ana,j}}{Y^o_{EG}} \tag{A.12}$$

$$q^{A,n}_{oxy,j} = \frac{Y_{EA}q^A_{ana,j}}{Y^o_{EA}} \tag{A.13}$$

This leads to a needed oxygen consumption rate, expressed in $mol_O\, g_X^{-1}\, h^{-1}$, in Eq. (A.16).

$$\Phi^{G,n}_{O,j} = Y_{OG}q^{G,n}_{oxy,j} \tag{A.14}$$

$$\Phi^{A,n}_{O,j} = Y_{OA}q^{A,n}_{oxy,j} \tag{A.15}$$

$$\Phi^n_{O,j} = \Phi^{G,n}_{O,j} + \Phi^{A,n}_{O,j} \tag{A.16}$$

Beside of the oxygen need, we estimate the oxygen availability which does not depend on the considered class and relies on liquid phase concentrations. This maximum possible oxygen consumption rate (upper-script p) is assumed to follow a Monod model. This model implements an inhibition of oxygen uptake rate by acetate as observed by Xu et al. (1999):

$$\Phi^p_O = \Phi^{\max}_O \frac{O}{O+K_O}\frac{K^O_{i,A}}{A+K^O_{i,A}} \tag{A.17}$$

If the oxygen availability excess the cell needs ($\Phi^p_O \geq \Phi^n_{O,j}$), then all energy is produced by oxidative pathway:

$$q^G_{oxy,j} = q^{G,n}_{oxy,j} \tag{A.18}$$

$$q^A_{oxy,j} = q^{A,n}_{oxy,j} \tag{A.19}$$

$$q^G_{ferm,j} = 0 \tag{A.20}$$

Otherwise, if oxygen is a limiting factor ($\Phi_O^p < \Phi_{O,j}^n$), the fermentative catabolism is triggered to fulfill energetic needs. Then, the fermentation reaction rate is deduced from the energy balance (Eq. (A.1)):

$$q_{oxy,j}^G = q_{oxy,j}^{G,n}\frac{\Phi_O^p}{\Phi_{O,j}^n} \tag{A.18′}$$

$$q_{oxy,j}^A = q_{oxy,j}^{A,n}\frac{\Phi_O^p}{\Phi_{O,j}^n} \tag{A.19′}$$

$$q_{ferm,j}^G = \frac{Y_{EG}q_{ana,j}^G - Y_{EG}^o q_{oxy,j}^G}{Y_{EG}^f} \tag{A.20′}$$

Using Eqs. (A.1)–(A.20)′, we define the function f introduced in Section 2.3.2:

$$f : [0,\mu_{\max}]\times\mathbb{R}_+^3 \longrightarrow \mathbb{R}^5$$
$$(\mu_j, G, A, O) \mapsto \left(q_{ana}^G, q_{ana}^A, q_{oxy}^G, q_{oxy}^A, q_{ferm}^G\right) \tag{A.21}$$

By using both this function and the calculation procedure of the overflow reaction rate, we may plot all the reaction rates throughout a population in a given environment as done in Fig. A1. This figure has been computed with the following concentrations: $G = 0.2\ g_G\ L^{-1}$, $O = 3.6\ mg_O\ L^{-1}$ and $A = 0.06\ g_A\ L^{-1}$. Some constants were also modified to make the figure more readable: $\mu_{\max}^G = 0.6\ h^{-1}$, $\mu_{\max}^A = 0.3\ h^{-1}$ and $\Phi_O^{\max} = 8\ mmol_O\ g_X^{-1}\ h^{-1}$.

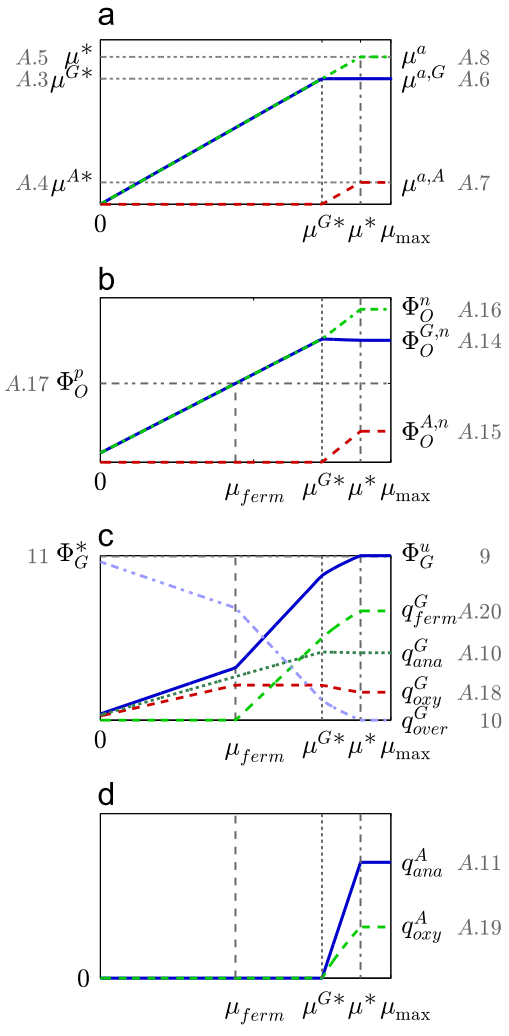

Fig. A1. Evolution of (a) growth rates, (b) oxygen uptake rates, (c) glucose uptake and reactions rates and (d) acetate reaction rates, throughout the population. Left hand side: legends of variables depending only on the environment (independent from individuals). Right hand side: legends for corresponding curves. Legends also detail the equations in which are given expressions of corresponding variables.

In this figure, each abscissa corresponds to the behavior of a particular class.

Fig. A1a shows the evolution of the actual growth rates both on glucose and acetate following Eqs. (A.6)–(A.8). Thus, three different regimes may be observed:

- $\mu_j \in [0;\mu^{G*}]$: only glucose in consumed due to strong internal limitations.
- $\mu_j \in [\mu^{G*},\mu^*]$: both glucose and acetate are consumed, but growth is still limited by internal capabilities.
- $\mu_j \in [\mu^*,\mu_{\max}]$: availabilities of glucose and acetate limit growth.

Fig. A1b shows the evolution of the needed oxygen consumption rate Φ_O^n, expressed in Eq. (A.16). When the oxygen needs (Φ_O^n) exceed the oxygen availability (Φ_O^p, Eq. (A.17)), the oxygen consumption is saturated and a part of the energy is produced through fermentation. It leads to the following regimes:

- $\mu_j \in [0;\mu_{ferm}]$: Energy produced only through the oxidative pathway.
- $\mu_j \in [\mu_{ferm},\mu_{\max}]$: Energy produced with both oxidative and fermentative pathways.

These two first sub-figures allow to identify, for each value of μ_j, what is (or are) the factor(s) limiting growth. From that, we can deduce the actual reaction rates, presented in Fig. A1c and d. In particular, these inter-correlations may be observed:

1. The anabolism rates, q_{ana}^G and q_{ana}^A, are directly proportional to $\mu^{a,G}$ (Eq. (A.10)) and $\mu^{a,A}$ (Eq. (A.11)).
2. The energy used for growth on acetate is always produced through acetate oxidation, then, q_{oxy}^A is directly proportional to q_{ana}^A.
3. The rate of energy production for growth on glucose are calculated such as the maximum part of this energy in produced through the oxidative pathway, in the limit of oxygen availabilities.
4. The useful part of glucose uptake, Φ_G^u is the sum of q_{ana}^G, q_{oxy}^G and q_{ferm}^G.
5. The overflow reaction rate, q_{over}^G, is defined as the difference between $\Phi_G^u(\mu^*)$ and $\Phi_G^u(\mu)$

Again, each abscissa represents the behavior of a particular class. It is important to note that depending on the state of the population, not all these behaviors will be exhibited. Our biological model couples the population balance with this metabolic model, leading to a wide variety of different possible behaviors at the scale of the population. In usual models, an instantaneous adaptation of bacteria to their environments is postulated. When using our metabolic model, such an hypothesis would constrain the observed behaviors to the one described in Fig. A1 at the μ^* abscissa.

Appendix B. Computation of the matrix of volume flow rates for the fedbatch reactor

Vrábel et al. (1999, 2000, 2001) designed, challenged and used a compartment model to run simulations compared with the behaviors observed within their large bioreactor (30 m^3). We used the description of their compartment model to compute the matrix of volume flow rates, M^f, needed to run our own

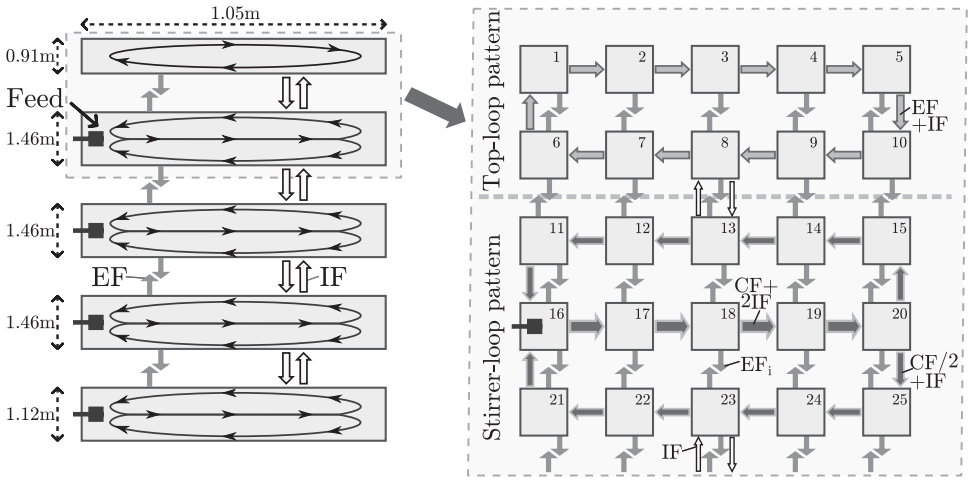

Fig. B1. Representation of the macroscopic flow patterns in the fedbatch reactor (left) and detail of its compartimentation and specific flows on the top of the reactor (right).

simulations. This model is based on the definition of three flows induced either by the use of Rushton turbines, or by the aeration.

Vrábel et al. observed that each of the four stirrers induces two circulation loops plus a supplementary loop on the top of the reactor as shown in Fig. B1 left. The flow in those loops is named Circulation Flow (CF). The presence of bubble for the aeration creates a flow that connects the circulation loops on their middles. This aeration Induced Flow (IF) also increases the velocity of the liquid within the circulation loops. Finally, the mixing and the aeration leads to the apparition of vertical turbulence flow (EF).

With these observations, Vrábel et al. modelized this hydrodynamics by splitting the reactor's volume in 14 rows (3 per stirrer plus 2 for the top-loop), and each row in 5 columns, as shown in the right of Fig. B1. The last figure shows a numeration of compartments as well as the flows going through each of them.

By definition, the matrix of volume flow rates is here a 70-by-70 matrix. Its value on the m-th row and n-th column represents the flow going from the compartment m to the compartment n. For example $M^f_{18,19} = CF + 2IF$ as shown in Fig. B1.

Once M^f has been designed based on values of CF, IF and EF, an estimation of these flows is needed. The calculation method used in estimating those flows has already been detailed by Vrábel et al. (1999, 2000). However, their procedure needs the knowledge of the stirrer speed and the gas-holdup throughout the culture. We then considered a constant stirrer speed of $1\ s^{-1}$, a gas flow of $1/60\ m^3\ s^{-1}$ and an overall gas-holdup of 8%. Those values are consistent with the range of values used by Vrábel et al. (1999, 2000, 2001).

These values lead to the following flows:

- $CF = 0.32\ m^3\ s^{-1}$
- $IF = 0.04\ m^3\ s^{-1}$
- $EF = 0.28\ m^3\ s^{-1}$

References

Altintas, M.M., Eddy, C.K., Zhang, M., McMillan, J.D., Kompala, D.S., 2006. Kinetic modeling to optimize pentose fermentation in *Zymomonas mobilis*. Biotechnol. Bioeng. 94 (2), 273–295.

Bezzo, F., Macchietto, S., Pantelides, C.C., 2003. General hybrid multizonal CFD approach for bioreactor modeling. AIChE J. 49 (8), 2133–2148.

Delafosse, A., Collignon, M.-L., Calvo, S., Delvigne, F., Crine, M., Thonart, P., Toye, D., 2014. CFD-based compartment model for description of mixing in bioreactors. Chem. Eng. Sci. 106 (0), 76–85.

Delafosse, A., Delvigne, F., Collignon, M.-L., Crine, M., Thonart, P., Toye, D., et al., 2010. Development of a compartment model based on CFD simulations for description of mixing in bioreactors. Biotechnol. Agron. Soc. Environ. 14 (2), 517–522.

Dhar, N., McKinney, J.D., 2007. Microbial phenotypic heterogeneity and antibiotic tolerance. Curr. Opin. Microbiol. 10 (1), 30–38.

Enfors, S.-O., Jahic, M., Rozkov, A., Xu, B., Hecker, M., Jürgen, B., Krüger, E., Schweder, T., Hamer, G., O'Beirne, D., Noisommit-Rizzi, N., Reuss, M., Boone, L., Hewitt, C., McFarlane, C., Nienow, A., Kovacs, T., Trägårdh, C., Fuchs, L., Revstedt, J., Friberg, P., Hjertager, B., Blomsten, G., Skogman, H., Hjort, S., Hoeks, F., Lin, H.-Y., Neubauer, P., van der Lans, R., Luyben, K., Vrábel, P., Manelius, Å., 2001. Physiological responses to mixing in large scale bioreactors. J. Biotechnol. 85 (2), 175–185 (Twenty years of the European Federation of Biotechnology).

Ferenci, T., 1996. Adaptation to life at micromolar nutrient levels: the regulation of *Escherichia coli* glucose transport by endoinduction and cAMP. FEMS Microbiol. Rev. 18 (4), 301–317.

Ferenci, T., 1999. Regulation by nutrient limitation. Curr. Opin. Microbiol. 2 (2), 208–213.

Franchini, A.G., Egli, T., 2006. Global gene expression in *Escherichia coli* K-12 during short-term and long-term adaptation to glucose-limited continuous culture conditions. Microbiology 152 (7), 2111–2127.

Henson, M.A., Müller, D., Reuss, M., 2002. Cell population modelling of yeast glycolytic oscillations. Biochem. J. 368 (2), 433–446.

Holms, H., 1996. Flux analysis and control of the central metabolic pathways in *Escherichia coli*. FEMS Microbiol. Rev. 19 (2), 85–116.

Hristov, H., Mann, R., Lossev, V., Vlaev, S., 2004. A simplified CFD for three-dimensional analysis of fluid mixing, mass transfer and bioreaction in a fermenter equipped with triple novel geometry impellers. Food Bioprod. Process. 82 (1), 21–34 (Mixing, Heat and Mass Transfer).

Lapin, A., Schmid, J., Reuss, M., 2006. Modeling the dynamics of *E. coli* populations in the three-dimensional turbulent field of a stirred-tank bioreactor—a structured—segregated approach. Chem. Eng. Sci. 61 (14), 4783–4797.

Larsson, G., Törnkvist, M., Wernersson, E., Trägårdh, C., Noorman, H., Enfors, S.-O., 1996. Substrate gradients in bioreactors: origin and consequences. Bioprocess. Biosyst. Eng. 14 (6), 281–289.

Leegwater, M.P.M., Neijssel, O.M., Tempest, D.W., 1982. Aspects of microbial physiology in relation to process control. J. Chem. Technol. Biotechnol. 32 (1), 92–99.

Lencastre Fernandes, R., Jensen, A.D., Nopens, I., Gernaey, K. V., 2013. The effect of bioreactor compartmentalization on yeast population dynamics during continuous cultivation. In: Proceedings of 5th International Conference on Population Balance Modelling, p. 5.

Lencastre Fernandes, R., Nierychlo, M., Lundin, L., Pedersen, A.E., Puentes Tellez, P.E., Dutta, A., Carlquist, M., Bolic, A., Schäpper, D., Brunetti, A.C., Helmark, S., Heins, A.L., Jensen, A.D., Nopens, I., Rottwitt, K., Szita, N., van Elsas, J.D., Nielsen, P.H., Martinussen, J., Sorensen, S.J., Lantz, A.E., Gernaey, K.V., 2012. Experimental methods and modeling techniques for description of cell population heterogeneity. Biotech. Adv. 29 (6), 575–599.

Linkès, M., Fede, P., Morchain, J., Schmitz, P., 2014. Numerical investigation of subgrid mixing effects on the calculation of biological reaction rates. Chem. Eng. Sci. 116, 473–485.

Mantzaris, N.V., 2005. A cell population balance model describing positive feedback loop expression dynamics. Comput. Chem. Eng. 29 (4), 897–909 (Control of Multiscale and Distributed Process Systems).

Mantzaris, N.V., 2006. Stochastic and deterministic simulations of heterogeneous cell population dynamics. J. Theor. Biol. 241 (3), 690–706.

Mantzaris, N.V., 2007. From single-cell genetic architecture to cell population dynamics: quantitatively decomposing the effects of different population heterogeneity sources for a genetic network with positive feedback architecture. Biophys. J. 92 (12), 4271–4288.

Matsuoka, Y., Shimizu, K., 2013. Catabolite regulation analysis of *Escherichia coli* for acetate overflow mechanism and co-consumption of multiple sugars based on systems biology approach using computer simulation. J. Biotechnol. 168 (2), 155–173 (Special Issue: Biotechnology for a healthy and green world).

Meadows, A.L., Karnik, R., Lam, H., Forestell, S., Snedecor, B., 2010. Application of dynamic flux balance analysis to an industrial *Escherichia coli* fermentation. Metab. Eng. 12 (2), 150–160 (Metabolic Flux Analysis for Pharmaceutical Production Special Issue).

Morchain, J., Fonade, C., 2009. A structured model for the simulation of bioreactors under transient conditions. AIChE J. 55 (11), 2973–2984.

Morchain, J., Gabelle, J.-C., Cockx, A., 2013. Coupling of biokinetic and population balance models to account for biological heterogeneity in bioreactors. AIChE J. 59 (2), 369–379.

Morchain, J., Gabelle, J.-C., Cockx, A., 2014. A coupled population balance model and CFD approach for the simulation of mixing issues in lab-scale and industrial bioreactors. AIChE J. 60 (1), 27–40.

Moullec, Y.L., Gentric, C., Potier, O., Leclerc, J., 2010. Comparison of systemic, compartmental and CFD modelling approaches: application to the simulation of a biological reactor of wastewater treatment. Chem. Eng. Sci. 65 (1), 343–350 (20th International Symposium in Chemical Reaction Engineering–Green Chemical Reaction Engineering for a Sustainable Future).

Natarajan, A., Srienc, F., 2000. Glucose uptake rates of single *E. coli* cells grown in glucose-limited chemostat cultures. J. Microbiol. Methods 42 (1), 87–96.

Nobs, J.-B., Maerkl, S.J., 2014. Long-term single cell analysis of *S. pombe* on a microfluidic microchemostat array. PLoS ONE 9 (April (4)), e93466.

Peskov, K., Mogilevskaya, E., Demin, O., 2012. Kinetic modelling of central carbon metabolism in *Escherichia coli*. FEBS J. 279 (18), 3374–3385.

Pirt, S.J., 1965. The maintenance energy of bacteria in growing cultures. Proc. R. Soc. B 163 (October), 224–231.

Ramkrishna, D., 2000. Population Balances: Theory and Applications to Particulate Systems in Engineering. Academic Press.

Russell, J.B., Cook, G.M., 1995. Energetics of bacterial growth: balance of anabolic and catabolic reactions. Microbiol. Rev. 59 (1), 48–62.

Ryall, B., Eydallin, G., Ferenci, T., 2012. Culture history and population heterogeneity as determinants of bacterial adaptation: the adaptomics of a single environmental transition. Microbiol. Mol. Biol. Rev. 76 (3), 597–625.

Varma, A., Boesch, B.W., Palsson, B.O., 1993. Stoichiometric interpretation of *Escherichia coli* glucose catabolism under various oxygenation rates. Appl. Environ. Microbiol. 59 (8), 2465–2473.

Vrábel, P., van der Lans, R., Cui, Y., Luyben, K., 1999. Compartment model approach: mixing in large scale aerated reactors with multiple impellers. Chem. Eng. Res. Des. 77 (4), 291–302.

Vrábel, P., vanderLans, R.G., Luyben, K.C., Boon, L., Nienow, A.W., 2000. Mixing in large-scale vessels stirred with multiple radial or radial and axial up-pumping impellers: modelling and measurements. Chem. Eng. Sci. 55 (23), 5881–5896.

Vrábel, P., vanderLans, R.G., vanderSchot, F.N., Luyben, K.C., Xu, B., Enfors, S.-O., 2001. CMA: integration of fluid dynamics and microbial kinetics in modelling of large-scale fermentations. Chem. Eng. J. 84 (3), 463–474.

Wang, Q., Ou, M.S., Kim, Y., Ingram, L., Shanmugam, K., 2010. Metabolic flux control at the pyruvate node in an anaerobic *Escherichia coli* strain with an active pyruvate dehydrogenase. Appl. Environ. Microbiol. 76 (7), 2107–2114.

Wick, L.M., Quadroni, M., Egli, T., 2001. Short- and long-term changes in proteome composition and kinetic properties in a culture of *Escherichia coli* during transition from glucose-excess to glucose-limited growth conditions in continuous culture and vice versa. Environ. Microbiol. 3 (9), 588–599.

Wick, L.M., Weilenmann, H., Egli, T., 2002. The apparent clock-like evolution of *Escherichia coli* in glucose-limited chemostats is reproducible at large but not at small population sizes and can be explained with monod kinetics. Microbiology 148 (9), 2889–2902.

Xu, B., Jahic, M., Blomsten, G., Enfors, S.-O., 1999a. Glucose overflow metabolism and mixed-acid fermentation in aerobic large-scale fed-batch processes with *Escherichia coli*. Appl. Microbiol. Biotechnol. 51 (5), 564–571.

Xu, B., Jahic, M., Enfors, S.-O., 1999. Modeling of overflow metabolism in batch and fed-batch cultures of *Escherichia coli*. Biotechnol. Progr. 15 (1), 81–90.

Zahradník, J., Mann, R., Fialová, M., Vlaev, D., Vlaev, S., Lossev, V., Seichter, P., 2001. A networks-of-zones analysis of mixing and mass transfer in three industrial bioreactors. Chem. Eng. Sci. 56 (2), 485–492 (16th International Conference on Chemical Reactor Engineering).